

Lensing in the Darkness: A Bayesian Analysis of 22 Chandra Sources at $z \gtrsim 6$ Shows No Evidence of Lensing

Fabio Pacucci^{1,2*}, Adi Foord^{3†}, Lucia Gordon⁴ and Abraham Loeb^{1,2}

¹*Center for Astrophysics | Harvard & Smithsonian, Cambridge, MA 02138, USA*

²*Black Hole Initiative, Harvard University, Cambridge, MA 02138, USA*

³*Kavli Institute of Particle Astrophysics and Cosmology, Stanford University, Stanford, CA 94305, USA*

⁴*Department of Physics, Harvard University, Cambridge, MA 02138, USA*

17 June 2022

ABSTRACT

More than 200 quasars have been detected so far at $z > 6$, with only one showing clear signs of strong gravitational lensing. Some studies call for a missing population of lensed high- z quasars, but their existence is still in doubt. A large fraction of high- z quasars being lensed would have a significant effect on the shape of the intrinsic quasar luminosity function (QLF). Here, we perform the first systematic search for lensed X-ray-detected quasars at $z \gtrsim 6$ employing a Bayesian analysis, with the code BAYMAX, to look for morphological evidence of multiple images that may escape a visual inspection. We analyzed a sample of 22 quasars at $z > 5.8$ imaged by the Chandra X-ray observatory and found none with statistically significant multiple images. In the sub-sample of the 8 sources with photon counts > 20 we exclude multiple images with separations $r > 1''$ and count ratios $f > 0.4$, or with separations as small as $0''.7$ and $f > 0.7$ at 95% confidence level. Comparing this non-detection with predictions from theoretical models suggesting a high and a low lensed fraction, we placed upper limits on the bright-end slope, β , of the QLF. Using only the sub-sample with 8 sources, we obtain, in the high-lensing model, a limit $\beta < 3.38$. Assuming no multiple source is present in the full sample of 22 sources, we obtain $\beta < 2.89$ and $\beta < 3.53$ in the high and low lensing models, respectively. These constraints strongly disfavor steep QLF shapes previously proposed in the literature.

Key words: gravitational lensing: strong – methods: statistical – surveys – quasars: supermassive black holes – X-rays: general

1 INTRODUCTION

Gravitational lensing alters the appearance of background astrophysical objects due to the presence of a mass distribution along the line of sight (see, e.g., the review by Schneider et al. 1992). In strong gravitational lensing (see, e.g., Treu 2010), a foreground object with a sufficiently large surface mass density distorts the light from a background source such as a quasar, leading to multiple images and a magnification of its brightness. Gravitational lensing is a powerful tool at the astronomer’s disposal, used to study the distribution of dark matter in clusters (e.g., Natarajan et al. 2017) and sub-structures (e.g., Meneghetti et al. 2020), to detect high-redshift sources otherwise too faint (e.g., Fan et al. 2019), to investigate the contribution of compact objects to dark matter (e.g., Alcock et al. 1996), and to constrain cosmological parameters (e.g., Wong et al. 2020).

In this study, we focus on the effect of gravitational lensing on quasars (Turner 1980), i.e. supermassive black holes that are accreting at large rates and luminosities (Schmidt 1968). Nowadays, tens of thousands of quasars have been discovered via systematic surveys (e.g., the Sloan Digital Sky Survey, Shen et al. 2011), even at very high- z (e.g., Fan et al. 2006; Mortlock et al. 2011; Wang et al. 2021). The detailed study of mass and redshift distribution of quasars is

relevant for a number of cosmological implications, including the origin of the first population of black holes (e.g., Haiman & Quataert 2004; Volonteri 2010; Haiman 2013; Gallerani et al. 2017; Woods et al. 2019; Inayoshi et al. 2020; Pacucci & Loeb 2022).

Although > 200 quasars are now detected at $z \sim 6$, remarkably only one lensed quasar at $z > 6$ was discovered (Fan et al. 2019): J0439+1634 at $z = 6.51$, with a possible magnification factor ~ 50 . Quasars at $z > 6$ are peculiar, as their emission at wavelengths shorter than that of the Lyman- α line (1216 Å) is absorbed by intervening neutral matter (Gunn & Peterson 1965). The fact that only one lensed quasar at $z > 6$ was discovered so far is interesting. Wyithe & Loeb (2002) predicted that up to 1/3 of quasars at $z > 6$ should be strongly magnified (by a magnification factor $\mu > 10$), due to the presence of galaxies along the line of sight. The lensing optical depth (Turner 1980; Hilbert et al. 2007), τ_L , is a measure of the probability that a source at redshift z_s is lensed by a lens at $z_l < z_s$. Intuitively, τ_L increases with z_s , as there are more potential lensing galaxies along the line of sight.

The discovery of the $z > 6$ lensed quasar J0439+1634 prompted a deeper look into selection criteria. Fan et al. (2019) argued that standard techniques based on the non-detection of the quasar at wavelengths shorter than the Lyman- α may cause a selection bias against lensed quasars. Additionally, multiply-imaged quasars at $z > 6$ might not be recognized as such due to the limited angular resolution of current telescopes (Pacucci & Loeb 2019). Recently, Yue et al. (2022)

* fabio.pacucci@cfa.harvard.edu

† foord@stanford.edu

revised the lensed fraction calculated by previous works, suggesting that improved accounting of the galaxy velocity dispersion functions would reduce the lensing probability by a factor of ~ 10 , shrinking the gap between theoretical predictions and actual observations of the lensed fraction.

Understanding the extent of the lensed population of $z > 6$ quasars is fundamental, as a large lensing fraction has profound effects on our measurements of the quasar luminosity function (QLF) and of the quasar mass function (e.g., Wyithe & Loeb 2002; Comerford et al. 2002). A large lensed fraction would cause a significant departure of the observed QLF from the intrinsic one, especially at its bright-end. Regarding the mass function, Fujimoto et al. (2020) claimed that the most massive quasar found at $z > 6$, with a mass $1.2 \times 10^{10} M_{\odot}$ (Wu et al. 2015), could be extremely magnified, and Pacucci & Loeb (2020) suggested that this would hint at a very large fraction of lensed high- z quasars. Further studies of the quasar proximity zone of this source ruled out extreme magnification (Davies et al. 2020). Additionally, the recent discovery of a putative physical pair of quasars at $z = 5.66$, separated by only 7.3 kpc (Yue et al. 2021) makes it even more urgent to better understand the role of lensing at $z \gtrsim 6$.

The value of the bright-end slope of the QLF is a powerful indicator of the lensing probability: larger values, corresponding to a steeper bright-end, would lead to a greater probability of quasars being lensed (Pei 1993, 1995; Comerford et al. 2002; Keeton et al. 2005). Pacucci & Loeb (2019) suggested that the probability of observing a gravitationally lensed quasar with magnification $\mu < 10$ is higher than the observed frequency of detections among the entire sample of $z > 6$ quasars.

In this study, we use Chandra X-ray data for 22 $z \gtrsim 5.8$ quasars to investigate the possibility that they are lensed, employing a Bayesian analysis performed with BAYMAX (Foord et al. 2019). In §2 we describe the gravitational lensing models employed, as well as BAYMAX. In §3 we describe the sample of Chandra sources used and the limitations of their analysis. Finally, in §4 and §5 we present our results and conclusions.

2 METHODOLOGY

This Section briefly describes the lensing models adopted as baseline for this work. The interested reader is referred to Pacucci & Loeb (2019) and Yue et al. (2022) for a more in-depth description. Additionally, we also describe BAYMAX, and the reader is referred to Foord et al. (2019, 2020) for a complete review of the code.

2.1 Gravitational Lensing Models

In this study we consider two different lensing models. The first, introduced by Pacucci & Loeb (2019), predicts a large fraction of lensed quasars at $z \sim 6$ and is in accordance with previous theoretical estimates (e.g., Wyithe & Loeb 2002; Comerford et al. 2002). For example, this model predicts a fraction of $\sim 20\%$ lensed quasars at $z \sim 6$, assuming a value $\beta = 3.6$ of the bright-end slope of the QLF. The second model, recently introduced by Yue et al. (2022) and in accordance with current observations, predicts a much lower fraction of lensed quasars at high- z . For comparison, this model predicts a fraction of $\sim 4\%$ lensed quasars at $z \sim 6$, again assuming $\beta = 3.6$. These two models differ significantly in the assumptions on the velocity dispersion of foreground galaxies, which act as lenses for the high- z quasars.

In order to easily distinguish between the two models, throughout

the remaining text we use the label `High Lensing` to describe the model in Pacucci & Loeb (2019), and `Low Lensing` to describe the model in Yue et al. (2022).

The interested reader is referred to the very broad descriptions of the models presented in Pacucci & Loeb (2019) and Yue et al. (2022) to better grasp the significance of the parameter β and its influence on the magnification bias and, hence, on the lensed fraction.

2.2 BAYMAX

This study makes use of BAYMAX (Foord et al. 2019), a code originally developed to analyze Chandra X-ray observations of Active Galactic Nuclei (AGN) and compute the likelihood that an object is better described by a single or a dual source model. While in the original interpretation of the results provided by BAYMAX the AGN would be a physical double system, with two super-massive black holes orbiting in the core of their merged galaxies, in our current interpretation the multiple images would be caused by gravitational lensing. Remarkably, the code is able to assign model probabilities for the source independently of the nature of the mechanism causing the multiple image. BAYMAX employs a Bayesian approach to calculate the best model to describe the source, once the Chandra's Point Spread Function (PSF) is properly taken into account.

Following the classic Bayesian statistical approach (see, e.g., Jeffreys 1935), we name D the available data. In our case, D is the distribution of photons of the AGN in the Chandra image, once it is corrected for PSF effects. Hence, the conditional probability of observing the data D given the model with a single source is indicated as $P(D|M_1)$ and, similarly, the conditional probability of observing the data D given the model with a double source is $P(D|M_2)$. Of course, both the single-source and the double-source models depend on additional parameters, which we generally indicate as θ_1 for the single source and θ_2 for the double source. In our case, these parameters are the angular distance between the two sources (r) and the count ratio (f , which represents the ratio between the number of counts associated with the secondary point source and the number of counts associated with the primary point source). Generally speaking, a larger angular separation between the two sources, as well as a count ratio near unity (i.e., equally bright sources) is more likely to result in a detection. In fact, if a source is gravitationally lensed, secondary X-ray images below a certain flux cannot be detected.

The Bayes factor (\mathcal{BF}), which is our primary indicator of the preference for one model or the other, is calculated by marginalizing over the entire parameter space of the models. Following Foord et al. (2019), the Bayes factor is then calculated as:

$$\mathcal{BF} = \frac{P(D|M_2, \theta_2) P(\theta_2, M_2) d\theta_2}{P(D|M_1, \theta_1) P(\theta_1, M_1) d\theta_1}. \quad (1)$$

As the Bayes factor is defined as the marginal probability of the model with a double source over the marginal probability of the model with a single source, $\ln \mathcal{BF} > 0$ indicates a preference for the double source model. BAYMAX calculates the Bayes factor using nested sampling (Skilling 2004) via the python package `nestle`¹ and uses `PyMC3` (Salvatier et al. 2016) for parameter estimation. We refer the reader to Foord et al. (2019, 2020) for a detailed discussion of the statistical techniques used to estimate likelihoods and posterior densities. Also, we note that BAYMAX is specifically designed to search for double images in Chandra data, while gravitational lensing can also produce quadrupole, or even higher order, images,

¹ <https://github.com/kbarbary/nestle>

although they are rarer than doubles. BAYMAX is generally able to detect multiplicity also in the case of a number > 2 of images.

The information provided by BAYMAX can be a strong indication of the multiplicity of a Chandra-detected source. In case of a suspected multiple source, this needs to be complemented by additional data to confirm gravitational lensing. First, higher resolution imaging, e.g. with the Hubble Space Telescope (HST) or the Atacama Large Millimeter/submillimeter Array (ALMA), could provide important information regarding the location of the multiple images. Also, a detection of a foreground object in the same line of sight would support the lensing hypothesis (see, e.g., Fan et al. 2019). The study of the properties of the lens would help in the definition of a lensing model that accounts for the relative magnifications and locations of the multiple images. Finally, the study of the quasar proximity zone and the derivation of the black hole mass from spectral lines could provide independent data on black hole growth rate, thus informing the lensing hypothesis (see, e.g., Davies et al. 2020).

3 DATA

In this Section we describe the Chandra data used in this study.

3.1 Chandra quasar sample

We use a sample of $z > 5.8$ quasars reported by Li et al. (2021). In particular, they analyze 152 quasars, including 46 with a $> 3\sigma$ detection by Chandra. Of these 152 quasars, 76 have $z > 5$, 35 have $z > 6$, and 2 have $z > 7$.

We restrict our analysis to Chandra observations with $z > 5.8$, with off-axis angles below $1'$ and non-zero values for the background-subtracted quasar counts in the $0.5 - 8$ keV energy range. The Chandra PSF becomes increasingly difficult to model as a function of increasing off-axis angles, and thus BAYMAX is most powerful (and sensitive to smaller separations and count ratios) when analysing on-axis observations. This results in 22 sources, where 16 have a single Chandra observation, 2 have 2 observations, 1 has 3 observations, 2 have 5 observations, and 1 has 11 observations. In Table 1 we list the observations used in our analysis for each source.

The Li et al. (2021) sample was chosen for the uniformity in its data analysis of Chandra sources, and because it provided a consistent catalog of high- z quasars. Table 2 includes the main descriptors of the data used, including the spectroscopic redshift, the net number of quasar counts in the energy range $0.5 - 8$ keV, as well as the reference to the discovery paper of each source (Fan et al. 2001, 2003, 2004, 2006; Willott et al. 2007, 2010; Venemans et al. 2015; Wu et al. 2015; Bañados et al. 2016; Tang et al. 2017; Mazzucchelli et al. 2017).

The angular resolution of the Chandra X-ray observatory is nominally $\sim 0''.5$, which is significantly worse than the HST with $\sim 0''.1$. In fact, the final confirmation that the $z = 6.51$ quasar J0439+1634 is lensed came from a high-resolution image obtained with the HST (Fan et al. 2019). The rationale for our choice of using Chandra sources for a search of lensed quasars is two pronged:

- (i) X-ray detected sources at high- z are most likely associated with quasar activity, i.e. with accretion on a super-massive black hole.
- (ii) BAYMAX adopts photon statistics and PSF analysis specifically designed for Chandra. The complex Bayesian analysis of Chandra images performed by BAYMAX allows the identification of multiple images of a source that, by eye inspection, looks single.

Yue et al. (2022) calculate the distribution of separations between multiple images in their model, obtaining that $\sim 85\%$ of lensed

Source name	Chandra Obs. ID	Exposure Time (s)
J002429+391318	20416	19700
J084035+562419	05613	15840
J022601+030259	20390	25900
J133550+353315	07783	23470
J111033-132945	20397	59330
...	22523	42840
...	22523	42840
...	23199	40630
...	23153	23990
...	23018	9980
J150941-174926	20391	26760
J162331+311200	05607	17210
J223255+293032	20395	54210
J005006+344522	20393	33490
J152637-205000	22233	39670
...	22165	32570
...	22231	29670
...	22232	21780
...	20469	16830
J141111+121737	05611	14270
J010013+290225	17087	14800
J163033+401209	05618	27390
J213233+121755	20417	17820
J000552-000655	05617	16930
J083643+005453	03359	5680
J160253+422824	05609	13200
J114816+525150	17127	77770
J164121+375520	21961	33480
...	20396	20830
J203209-211402	21725	73370
...	20470	44480
...	21726	33070
J103027+052455	19987	126380
...	20045	61270
...	19926	49420
...	18185	46330
...	18187	40400
...	20046	36590
...	18186	34620
...	19994	32650
...	19995	26720
...	20081	24910
...	03357	7950
J130608+035626	03358	118240
...	03966	8160

Table 1. Summary of the Chandra data of the 22 $z \gtrsim 5.8$ sources studied. From left to right: the source name, Chandra observation ID, and exposure time of Chandra observation.

quasars at $z = 6$ should have angular separations $> 0''.5$, and hence larger than the angular resolution of Chandra. Note that this is comparable to the fraction calculated in Pacucci & Loeb (2019) at $z = 6.5$. However, the detectability of any putative lensed system via BAYMAX will strongly rely on the total number of counts, the separation, and the count ratio (e.g., below ~ 10 counts, it is difficult to find dual X-ray point sources with BAYMAX at high significance for most of parameter space). In Section 4.2 we review our sensitivity in parameter space for the sample, as a function of their total counts.

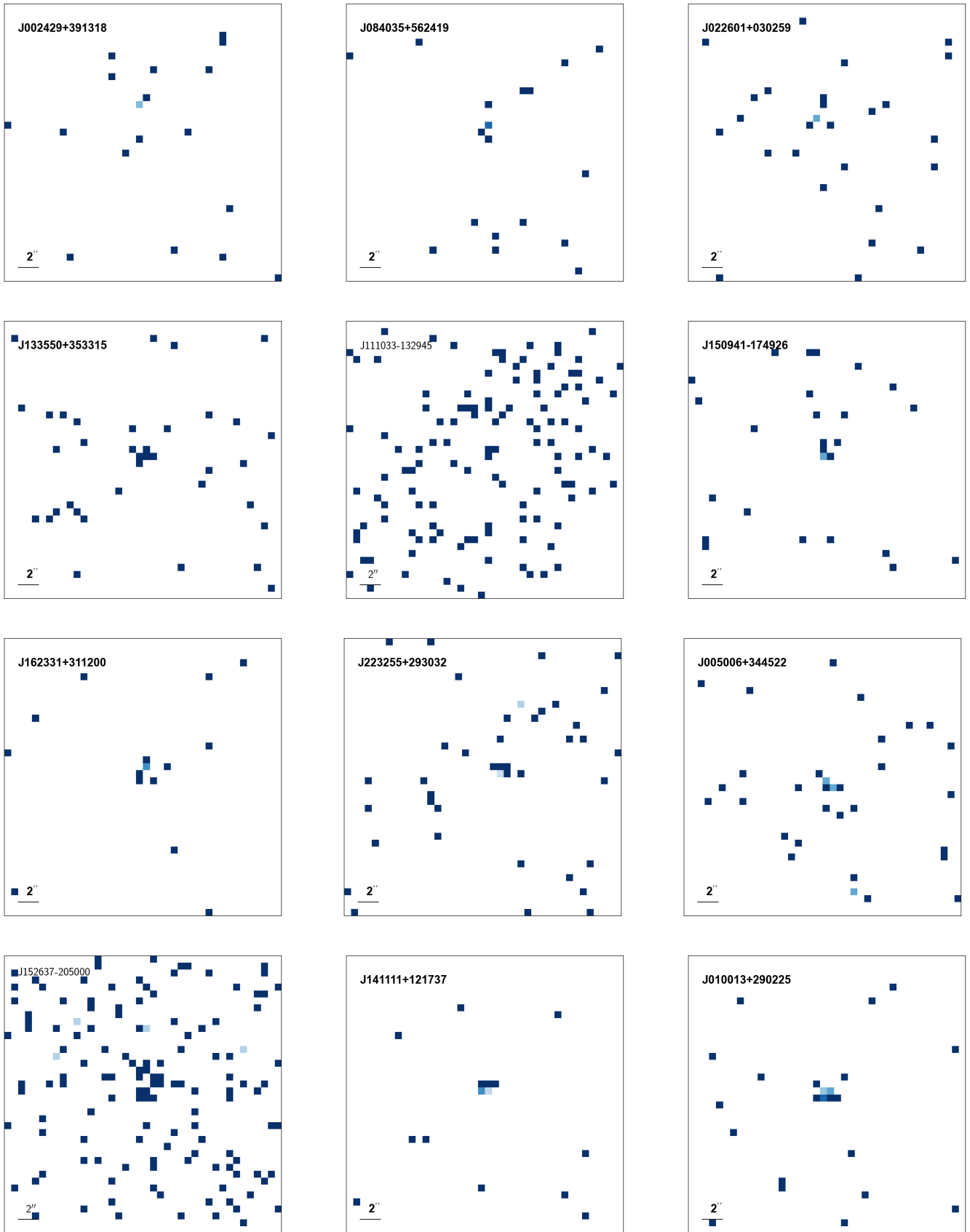


Figure 1. Binned X-ray images of selected sources in our dataset. Photons have energies in the range 0.5 – 8 keV, and the scale is 0.5'' per pixel.

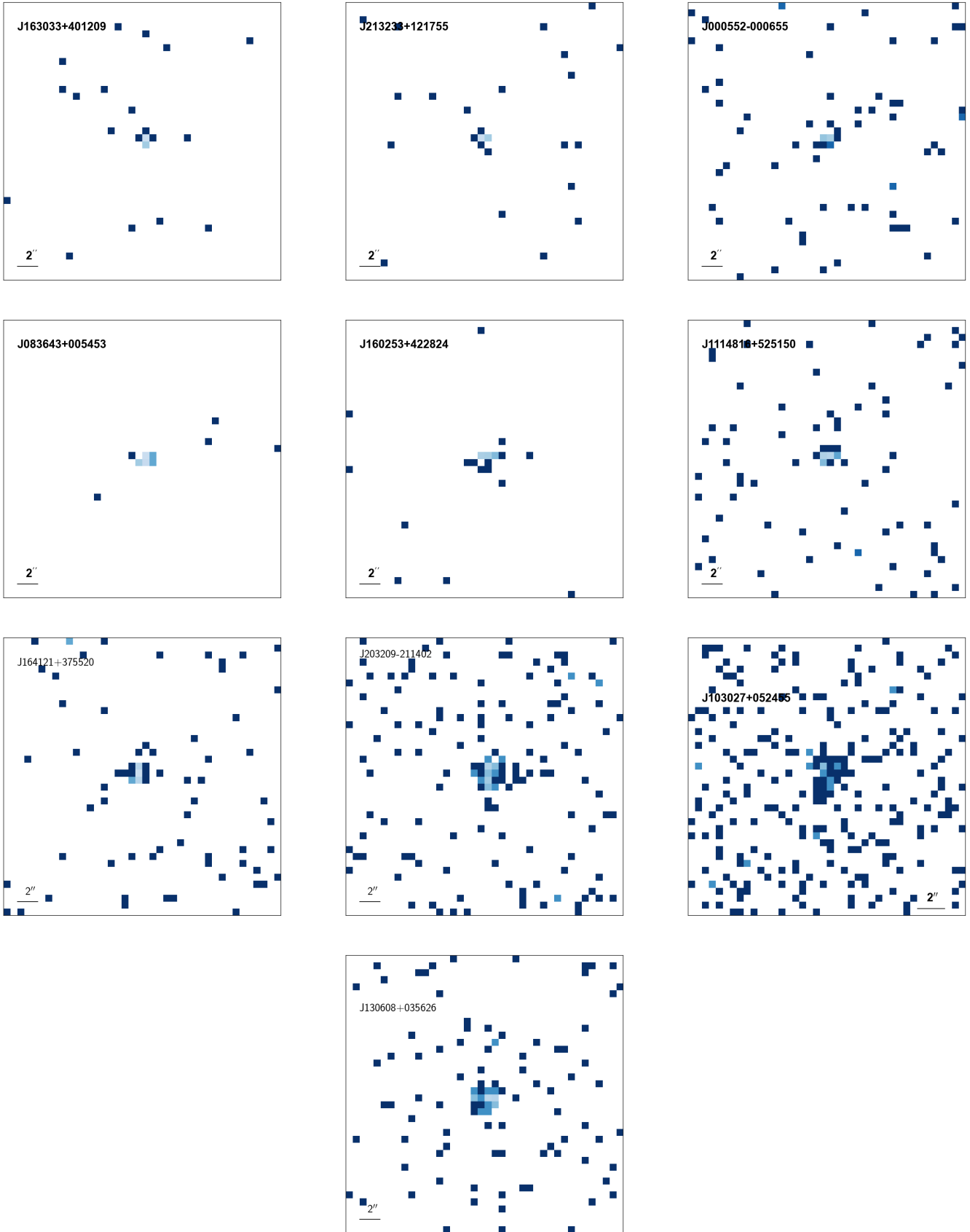


Figure 2. Binned X-ray images of selected sources in our dataset. Photons have energies in the range 0.5 – 8 keV, and the scale is 0.5'' per pixel.

Source name	α	δ	Redshift	X-ray Counts	$\ln \mathcal{BF}$	Reference
J002429+391318	00:24:29.77	+39:13:18.98	6.621	3	0.12 ± 0.25	Tang et al. (2017)
J084035+562419	08:40:35.09	+56:24:19.90	5.816	4	0.15 ± 0.31	Fan et al. (2006)
J022601+030259	02:26:01.88	+03:02:59.40	6.541	5	0.61 ± 0.23	Venemans et al. (2015)
J133550+353315	13:35:50.806	+35:33:15.80	5.901	6	0.13 ± 0.27	Fan et al. (2006)
J111033-132945	11:10:33.98	-13:29:45.60	6.515	6	0.18 ± 0.49	Venemans et al. (2015)
J150941-174926	15:09:41.78	-17:49:26.80	6.123	6	-0.01 ± 0.29	Willott et al. (2007)
J162331+311200	16:23:31.81	+31:12:00.50	6.254	7	0.11 ± 0.27	Fan et al. (2004)
J223255+293032	22:32:55.15	+29:30:32.20	6.666	8	0.07 ± 0.27	Venemans et al. (2015)
J005006+344522	00:50:06.67	+34:45:22.60	6.251	9	0.21 ± 0.32	Willott et al. (2010)
J152637-205000	15:26:37.84	-20:50:00.80	6.586	14	0.43 ± 0.47	Mazzucchelli et al. (2017)
J141111+121737	14:11:11.29	+12:17:37.4	5.854	13	-0.07 ± 0.36	Fan et al. (2004)
J010013+290225	01:00:13.02	+28:02:25.80	6.327	14	-0.15 ± 0.37	Wu et al. (2015)
J163033+401209	16:30:33.90	+40:12:09.60	6.066	14	-0.01 ± 0.32	Fan et al. (2003)
J213233+121755	21:32:33.19	+12:17:55.46	6.588	15	-0.06 ± 0.31	Mazzucchelli et al. (2017)
J000552-000655	00:05:52.34	-00:06:55.80	5.844	21	0.07 ± 0.26	Fan et al. (2004)
J083643+005453	08:36:43.86	+00:54:53.23	5.834	24	-0.18 ± 0.33	Fan et al. (2001)
J160253+422824	16:02:54.18	+42:28:22.90	6.083	27	-0.22 ± 0.39	Fan et al. (2004)
J114816+525150	11:48:16.65	+52:51:50.21	6.419	35	-0.04 ± 0.34	Fan et al. (2003)
J164121+375520	16:41:21.64	+37:55:20.50	6.047	45	0.53 ± 0.41	Willott et al. (2007)
J203209-211402	20:32:09.99	-21:14:02.31	6.234	72	-0.77 ± 0.48	Banados et al. (2016)
J103027+052455	10:30:27.10	+05:24:55.00	6.280	132.325	0.31 ± 0.66	Fan et al. (2001)
J130608+035626	13:06:08.26	+03:56:26.35	6.034	132	0.42 ± 0.43	Fan et al. (2001)

Table 2. Summary of the properties of the 22 $z \gtrsim 5.8$ Chandra sources studied. From left to right: the source name, redshift, background-subtracted quasar counts (0.5 – 8 keV) across all observations, computed Bayes factor, and original reference for the source. We denote the 3 count bins used for our sensitivity tests with horizontal line breaks (see 4.2).

4 RESULTS

We are now in a position to discuss the results of our analysis performed with `BAYMAX`, and their consequences for the QLF.

4.1 Results of the `BAYMAX` Analysis

For each quasar, we restrict our analysis to photons with energies between 0.5–8 keV. We analyze the photons contained within $20'' \times 20''$ rectangular regions that are centered on the nominal X-ray coordinates of the quasar (see Figure 1 and 2). We run `BAYMAX` using non-informative priors, where the prior distributions for location of the primary and secondary X-ray point source are uniform distributions bound in the x- and y-direction between the full extent of the $20'' \times 20''$ field of view. For quasars with multiple observations, `BAYMAX` models the PSF of each observation and calculates the likelihoods for each observation individually and then fits for astrometric shifts between different observations of the same source.

We ran `BAYMAX` 100 times on each of the 22 quasars reported in Table 2, with the exception of J111033-132945, J152637-205000, J103027+052455, and J130608+035626. The reason to run the code a large number of times is that the choice of the parameters of the models is, by definition, stochastic. Hence, the computed Bayes factor is never exactly the same and an averaging process over a large number of runs is necessary to obtain accurate results, including an appropriate description of the confidence intervals.

For J111033-132945, J152637-205000, J103027+052455, and J130608+035626, the computational time necessary to evaluate the sources 100 times was exceptionally large, a result of the total number of counts and/or number of observations per source. For these sources, we instead quote the statistical error bars returned from `nestle` on a single-run. The errors provided by `nestle` are calculated for each model, at each iteration, and are assumed to be

proportional to the ratio of the “information” to the number of live points (see Skilling 2004 for explicit details). In the past, we have found that the statistical error bars returned from `nestle` are consistent with the 1σ spread in the $\ln \mathcal{BF}$ values when running `BAYMAX` 100 times on a single source (Foord et al. 2020, 2021).

In Table 2 we list the average $\ln \mathcal{BF}$ and the 1σ error bar for each quasar. We find that all of the sources have $\ln \mathcal{BF}$ values consistent with 0 within the 1σ error bar, indicative that *there is no strong evidence for a lensed quasar in our sample*. In the next §4.2 we discuss the search sensitivity, which is crucial to correctly interpret this result.

4.2 Search Sensitivity

Considering that this paper presents the first use of `BAYMAX` to study lensed sources at very high-redshift and with low photon counts, we perform a full analysis of the sensitivity of this search.

For a given number of total counts, `BAYMAX` will be insensitive to multi-point sources at the low-end of separation and count ratio space. For example, for on-axis Chandra observations with > 700 counts between 0.5–8 keV, we can expect that `BAYMAX` will be sensitive to dual point sources with count ratios greater than 0.2, down to separations as low as $0''.3$ (Foord et al. 2019). However, at the low-end of the count range, `BAYMAX` may not be able to discern a single point source from multiple point sources across a wider range of count ratio and separation values.

We measure the sensitivity of `BAYMAX` across our sample to quantify how well `BAYMAX` can correctly identify a putative lensed quasar, at a given separation and count ratio. Because the sensitivity of `BAYMAX` is directly tied to the total number of counts associated with a source, we divide our sample into 3 bins based on total number of 0.5–8 keV counts and analyze the sensitivity of `BAYMAX` for the

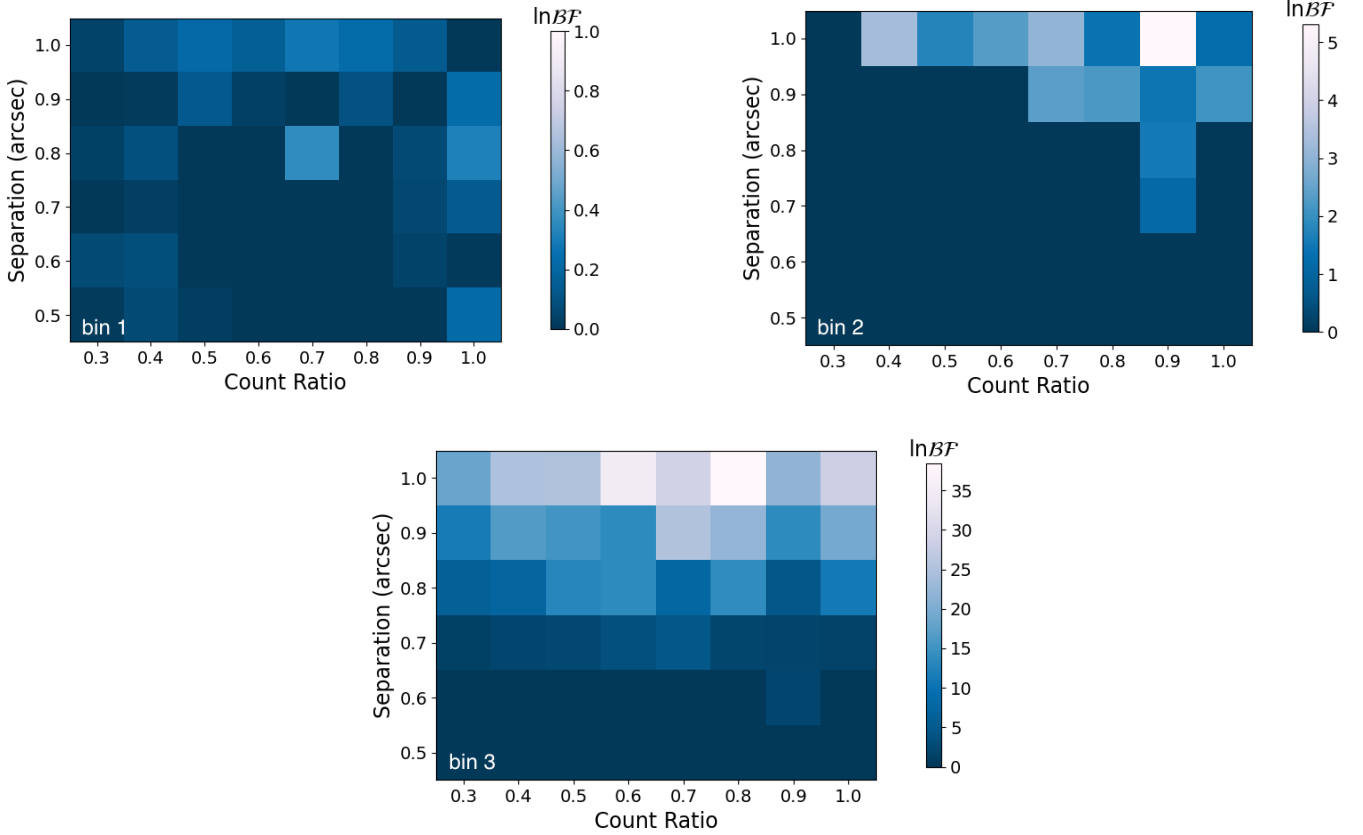


Figure 3. Results of the feasibility analysis described in Sec. 4.2. We show the sensitivity of BAYMAX to detect dual X-ray point sources in 3 count bins, as a function of separation (r) and count ratio (f). For our lowest count bin (average 9 counts), we are not sensitive to detecting dual X-ray point sources over most of parameter space. However, for bin 2 (average of 38 counts) at typical separations $r \geq 1''$ we obtain Bayes factors that are compatible with a significant (at the 95% confidence level, C.L.) detection; for bin 3 (average of 132 counts) at typical separations $r \geq 0''.7$ we obtain Bayes factors that are compatible with a significant (at the 95% C.L.) detection.

average number of counts per bin. In Table 2 we denote the sources in each bin via horizontal line breaks; bin 1 has fourteen sources with 3–15 counts, bin 2 has six sources with 21–72 counts, and bin 3 has two sources with >100 counts.

We simulate dual X-ray point sources across r – f space that have, on average, 9 (bin 1), 38 (bin 2), or 132 (bin 3) counts between 0.5–8 keV. We simulate systems with separations that range between $0''.5$ – $1''$ and count ratios that range between 0.3–1. For each r – f point in the parameter space, we evaluate simulations with randomized position angles between the primary and secondary X-ray point source. Our results are shown in Figure 3, where we plot the mean $\ln \mathcal{BF}$ for each point in the parameter space.

For each count bin, we define regions of parameter space where BAYMAX cannot statistically differentiate between a single and multiple point source wherever the mean $\ln \mathcal{BF}$ is consistent with 0 at the 95% confidence interval. This allows us to quantify regions in parameter space where each quasar is consistent with emission from a single X-ray point source. Consistent with expectations, BAYMAX favors the dual point source model more strongly as the separation and count ratio increase, and is capable of probing smaller separations for a given count ratio as the total number of counts increase. For bin 1, we find that at all count ratio and separation bins the mean $\ln \mathcal{BF}$ is consistent with 0. For bin 2, we find that at $r \geq 1''$ we are sensitive to duals at $f \geq 0.4$ and we can statistically probe separations as small as $0''.7$ at $f > 0''.7$. Lastly, for bin 3, at $r \geq 0''.7$ we

are statistically sensitive to dual X-ray point sources across the entire f -space.

Thus, for the majority of this sample (which reside in count bin 1), there is not enough data to claim at the 95% confidence interval that the emission from the quasar is consistent with single X-ray point source. However, at the 95% C.L. we conclude that none of the quasars in bin 2 are dual at $r \geq 1''$ for $f \geq 0.4$ and none of the quasars in bin 3 are dual at $r \geq 0''.7$ for $f > 0.3$.

Carrying out simulations of dual X-ray point sources across r – f space, while varying the total number of counts, we find that we are sensitive to detecting multiple X-ray point sources across most of f space to separations as low as $0''.5$, with at least 200 counts (see Figure 4). To reach this sensitivity for each source, observations between $1.5\times$ (at the low-end, for J130608+035626 and J103027+052455) to $67\times$ (at the high-end, for J002429+391318) deeper are necessary, with the average observation needing to be $14\times$ deeper. Given our average exposure time of 26 ks, such observations are not easily feasible with follow-up Chandra observations. Alternatively, if each source in our sample was between 1.5 – 67 times brighter, the archival data sets would allow for a more sensitive study.

4.3 Constraining the Shape of the Quasar Luminosity Function

We now proceed to place some constraints on the value of the β parameter for the QLF at $z \sim 6$.

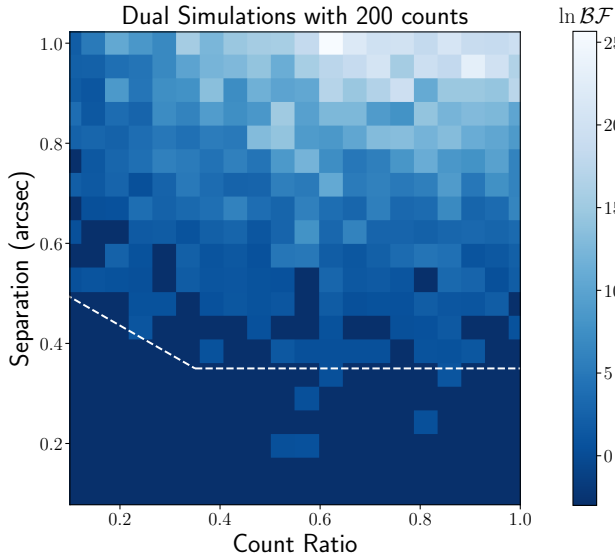


Figure 4. Bayes factors for simulated dual AGN with 200 total counts, with varying separation (in arcseconds) and count ratios. For each point in the parameter space, we evaluated 100 simulations with randomized position angles (0–360 deg) between the primary and secondary image. Here we display the logarithm of the mean \mathcal{BF} for each point in the parameter space. We enforce a cut of $\ln \mathcal{BF} > 3$, where above this value the Bayes factor is classified as strongly in favor of the dual point source model. Points in the parameter space with a $\ln \mathcal{BF}$ below this value are displayed in dark blue. With 200 counts between 0.5–8 keV, BAYMAX is capable of correctly identifying multiple AGN at flux ratios as low as $f = 0.1$ down to separations of $0''.5$. To reach this sensitivity for our sample, observations between 1.5 to 67 times deeper are necessary.

As mentioned in §3, Yue et al. (2022) calculate that $\sim 85\%$ of sources at $z \sim 6$ should have a sufficient separation between images to be detected above the resolution limit $\varphi_{\text{lim}} \sim 0''.5$ of the Chandra X-ray telescope (see a similar calculation at $z \approx 6.5$ also in Pacucci & Loeb 2019). We call this probability $P(\varphi > \varphi_{\text{lim}})$. Additionally, for each value of β in the range $[2, 4]$, we can use the High Lensing model and the Low Lensing model to compute the lensed fraction $P(\beta)$. Hence, the fraction of N sources with sufficient angular separation to be observed as multiples by Chandra, $N \times P(\varphi > \varphi_{\text{lim}})$, is multiplied by the probability $P(\beta)$, for values of β in the range $[2, 4]$, thus obtaining Fig. 5.

In this figure we show with a solid line the expected number of multiple sources in the sample of $N = 8$ Chandra-detected quasars with the highest photon counts, as a function of the parameter β . The sources with the highest photon number counts, reported in Table 2, are the only ones for which we can exclude multiplicity, following our analysis with BAYMAX. As we cannot claim any multiple source with high significance in this reduced dataset, the number of observed lensed quasars is $N_{\text{obs}} < 1$. This model leads to an upper limit of $\beta < 3.38$, which excludes at 95% C.L. the value of $\beta = 3.6$ (Yang et al. 2016) commonly used in the literature. Unfortunately, only 8 sources are not sufficient to place any meaningful upper limit with the Low Lensing model.

Considering the full sample of $N = 22$ sources, we can also calculate constraints on β , in the assumption that none of them are multiple. This translates in the following *upper limits* on β :

- $\beta < 2.89$ in the High Lensing model
- $\beta < 3.53$ in the Low Lensing model

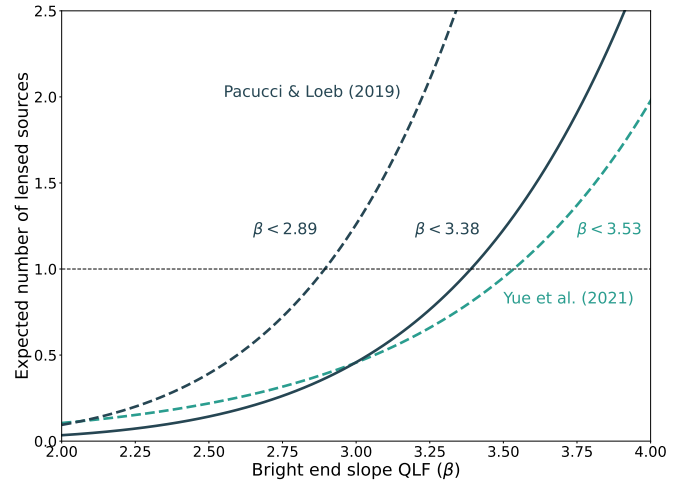


Figure 5. Expected number of multiple sources in our sample, as a function of the bright-end slope, β , of the QLF. Predictions are based on the High Lensing model (dark blue) and the Low Lensing model (green) as described in the main text. Considering only the 8 sources pertaining to the two bins with the highest count numbers, we obtain an upper limit of $\beta < 3.38$ in the High Lensing model, while the Low Lensing model is not constraining. With no detection of multiple sources out of the full sample of 22 sources (dashed lines), we obtain a constraint of $\beta < 2.89$ with the High Lensing model, and $\beta < 3.53$ with the Low Lensing model.

The stricter upper limit rules out the commonly used value of $\beta = 3.6$ (Yang et al. 2016), while it is compatible with the shallower value of $\beta = 2.8$ (Jiang et al. 2016). The looser upper limit also excludes $\beta = 3.6$. Finally, note that overall our study significantly rules out steeper values of the bright-end slope of the QLF, e.g., $\beta \approx 5$ (Kulkarni et al. 2019).

Assuming $\beta \approx 2.8$, a value that is widely used in the literature (e.g., Jiang et al. 2016) and in accordance with our limits, the probability of a $z \sim 6$ quasar being lensed is estimated to be approximately 2% and 4% by the Low Lensing and High Lensing models, respectively. Assuming that all our observations meet the count threshold (>200 counts between 0.5–8 keV) necessary for a sensitivity down to separations of $0''.5$, we estimate that we would need a sample size between 14–27 high- z AGN to have $>10\%$ chance of detecting 1 or more lensed AGN (assuming binomial statistics). The sample size increases to be between 42–84 high- z AGN to have $>50\%$ chance of detecting 1 or more lensed AGN. Given the large exposure times necessary to detect >200 counts for high- z AGN with Chandra, such a project is likely not currently feasible. However, future X-ray telescopes with similar (or better) angular resolution to Chandra, but larger sensitivity, may allow for such an observing project. The probe-class mission concept Advanced X-ray Imaging Satellite (AXIS), for example, will have a collecting area about an order of magnitude larger than Chandra (Mushotzky 2018; Koss et al. 2019).

5 DISCUSSION AND CONCLUSIONS

In this study we have investigated 22 X-ray detected quasars at $z > 5.8$ with BAYMAX, a code designed to perform a Bayesian analysis of multiple sources, whether the multiple images are physical or caused by gravitational lensing. Our goal was to study the lensed fraction of high- z quasars, after the discovery of the first strongly lensed quasar by Fan et al. 2019.

Out of 22 sources, we could not confirm any statistically significant multiple image. For the 8 sources with a photon count number > 20 , we can rule out at 95% C.L. that they have multiple images with separations larger than $1''$ and count ratios $f > 0.4$. While some of the sources analyzed were flagged by BAYMAX as possessing a slight preference for the multiple image model, all of them were statistically compatible with the single model.

This non-detection allows us to constrain the bright-end slope of the QLF at $z \sim 6$. With only the $N = 8$ sources pertaining in the two highest count bins, we obtain an upper limit of $\beta < 3.38$ with the High Lensing model. Considering $N = 22$ sources, we obtain $\beta < 2.89$ in the High Lensing model and $\beta < 3.53$ in the Low Lensing model. These upper limits significantly rule out extreme values of β recently proposed in the literature (e.g., $\beta \approx 5$, Kulkarni et al. 2019), and point to much shallower values (e.g., $\beta = 2.8$, Jiang et al. 2016).

Is it surprising that we found no clear sign of lensed quasars in our sample of $z \gtrsim 6$ sources? Possibly not. Some of the possible reasons to explain why we found none are the following:

- (i) Higher photon counts are needed, requiring deeper Chandra observations, next-generation X-ray telescopes, or brighter sources.
- (ii) Larger source samples are needed.
- (iii) The lensed fraction of high- z quasars is lower than previously predicted (Yue et al. 2022).

Regarding (i), our search sensitivity analysis with BAYMAX (see Sec. 4.2) showed that we need photon counts > 20 to be able to discriminate sources with separations $r > 1''$ and count ratios $f > 0.4$ at 95% C.L.; unfortunately, only $\sim 36\%$ of the sources in our sample met this criterion. Deeper Chandra observations of known quasars, or a sample selection of only the X-ray brightest sources, can improve the statistics for future studies of this kind.

Additionally, we chose a uniform sample of 22 Chandra-detected sources which are on-axis and some of them with multiple observations. By expanding the sample significantly, we might have ended up with a statistically significant detection. For example, Yue et al. (2022) predicts that there should be ~ 15 gravitationally lensed quasars at $z > 6$ currently detectable (in optical wavelengths, at least) in the whole sky.

Ultimately, it is possible that previous theoretical models (e.g. Wyithe & Loeb 2002; Comerford et al. 2002; Pacucci & Loeb 2019) over-estimated the lensed fraction of quasars at $z \sim 6$. Recently, Yue et al. (2022) suggested that the lensed fraction could be ~ 10 times lower than previously predicted, explaining the observational detection of a single lensed quasar in the epoch of reionization thus far (Fan et al. 2019). This would suggest the necessity to re-evaluate the velocity dispersion function of galaxies at $z \lesssim 3$, i.e. where most of the lensing sources are. In fact, Yue et al. (2022) show that the observed low number of lensed quasars at $z > 6$ can be explained by using the locally observed velocity dispersion function at $z < 0.1$ (Sohn et al. 2017; Hasan & Crocker 2019). Previous studies may have thus over-estimated the available lensing power at $z \lesssim 3$.

Upcoming optical surveys such as Euclid and the LSST will greatly expand our reach in the study of lensed quasars at $z > 6$, and will most likely solve the long-lasting controversy over the lensed fraction. The expansion of our search of lensed quasars to optically-observed sources would require a substantial re-purposing of BAYMAX, to include statistics able to deal with very high photon counts. The possibilities opened up by a Bayesian analysis of a quasar image, when compared to a visual inspection, are worth investigating in the near future. Whatever route we take, it is most likely that with upcoming optical and X-ray surveys of the sky the multi-decadal

question of how likely it is for a high- z quasar to be strongly lensed will soon be solved.

ACKNOWLEDGEMENTS

We thank the anonymous referee for constructive comments on the manuscript. F.P. acknowledges support from a Clay Fellowship administered by the Smithsonian Astrophysical Observatory. This work was supported by the Black Hole Initiative at Harvard University, which is funded by grants from the John Templeton Foundation and the Gordon and Betty Moore Foundation. A.F. acknowledges support by the Porat Postdoctoral Fellowship at Stanford University.

DATA AVAILABILITY

The code BAYMAX is proprietary. The scripts used to analyze the data will be shared on reasonable request to the corresponding authors.

REFERENCES

- Alcock C., et al., 1996, *ApJ*, 471, 774
 Bañados E., et al., 2016, *ApJS*, 227, 11
 Comerford J. M., Haiman Z., Schaye J., 2002, *ApJ*, 580, 63
 Davies F. B., Wang F., Eilers A.-C., Hennawi J. F., 2020, *ApJ*, 904, L32
 Fan X., et al., 2001, *AJ*, 122, 2833
 Fan X., et al., 2003, *AJ*, 125, 1649
 Fan X., et al., 2004, *AJ*, 128, 515
 Fan X., et al., 2006, *AJ*, 131, 1203
 Fan X., et al., 2019, *ApJ*, 870, L11
 Foord A., et al., 2019, *ApJ*, 877, 17
 Foord A., Gültekin K., Nevin R., Comerford J. M., Hodges-Kluck E., Barrows R. S., Goulding A. D., Greene J. E., 2020, *ApJ*, 892, 29
 Foord A., Gültekin K., Runnoe J. C., Koss M. J., 2021, *ApJ*, 907, 71
 Fujimoto S., Oguri M., Nagao T., Izumi T., Ouchi M., 2020, *ApJ*, 891, 64
 Gallerani S., Fan X., Maiolino R., Pacucci F., 2017, *Publ. Astron. Soc. Australia*, 34, e022
 Gunn J. E., Peterson B. A., 1965, *ApJ*, 142, 1633
 Haiman Z., 2013, in Wiklind T., Mobasher B., Bromm V., eds, *Astrophysics and Space Science Library Vol. 396, The First Galaxies*. p. 293 ([arXiv:1203.6075](https://arxiv.org/abs/1203.6075)), doi:10.1007/978-3-642-32362-1_6
 Haiman Z., Quataert E., 2004, in Barger A. J., ed., *Astrophysics and Space Science Library Vol. 308, Supermassive Black Holes in the Distant Universe*. p. 147 ([arXiv:astro-ph/0403225](https://arxiv.org/abs/astro-ph/0403225)), doi:10.1007/978-1-4020-2471-9_5
 Hasan F., Crocker A., 2019, arXiv e-prints, p. [arXiv:1904.00486](https://arxiv.org/abs/1904.00486)
 Hilbert S., White S. D. M., Hartlap J., Schneider P., 2007, *MNRAS*, 382, 121
 Inayoshi K., Visbal E., Haiman Z., 2020, *ARA&A*, 58, 27
 Jeffreys H., 1935, *Proceedings of the Cambridge Philosophical Society*, 31, 203
 Jiang L., et al., 2016, *ApJ*, 833, 222
 Keeton C. R., Kuhlen M., Haiman Z., 2005, *ApJ*, 621, 559
 Koss M., et al., 2019, *Astro2020: Decadal Survey on Astronomy and Astrophysics*, 2020, 504
 Kulkarni G., Worbeck G., Hennawi J. F., 2019, *MNRAS*, 488, 1035
 Li J.-T., Wang F., Yang J., Bregman J. N., Fan X., Zhang Y., 2021, *MNRAS*, 504, 2767
 Mazzucchelli C., et al., 2017, *ApJ*, 849, 91
 Meneghetti M., et al., 2020, *Science*, 369, 1347
 Mortlock D. J., et al., 2011, *Nature*, 474, 616
 Mushotzky R., 2018, in den Herder J.-W. A., Nikzad S., Nakazawa K., eds, *Society of Photo-Optical Instrumentation Engineers (SPIE) Conference Series Vol. 10699, Space Telescopes and Instrumentation 2018: Ultraviolet to Gamma Ray*. p. 1069929 ([arXiv:1807.02122](https://arxiv.org/abs/1807.02122)), doi:10.1117/12.2310003

- Natarajan P., et al., 2017, *MNRAS*, 468, 1962
Pacucci F., Loeb A., 2019, *ApJ*, 870, L12
Pacucci F., Loeb A., 2020, *ApJ*, 889, 52
Pacucci F., Loeb A., 2022, *MNRAS*, 509, 1885
Pei Y. C., 1993, *ApJ*, 403, 7
Pei Y. C., 1995, *ApJ*, 440, 485
Salvatier J., Wiecki T., Fonnesbeck C., 2016, *PeerJ Computer Science*, 2
Schmidt M., 1968, *ApJ*, 151, 393
Schneider P., Ehlers J., Falco E. E., 1992, *Gravitational Lenses*,
[doi:10.1007/978-3-662-03758-4](https://doi.org/10.1007/978-3-662-03758-4).
Shen Y., et al., 2011, *ApJS*, 194, 45
Skilling J., 2004, in Fischer R., Preuss R., Toussaint U. V., eds, *American Institute of Physics Conference Series Vol. 735*, American Institute of Physics Conference Series. pp 395–405, [doi:10.1063/1.1835238](https://doi.org/10.1063/1.1835238)
Sohn J., Zahid H. J., Geller M. J., 2017, *ApJ*, 845, 73
Tang J.-J., et al., 2017, *MNRAS*, 466, 4568
Treu T., 2010, *ARA&A*, 48, 87
Turner E. L., 1980, *ApJ*, 242, L135
Venemans B. P., et al., 2015, *ApJ*, 801, L11
Volonteri M., 2010, *Astronomy and Astrophysics Review*, 18, 279
Wang F., et al., 2021, *ApJ*, 907, L1
Willott C. J., et al., 2007, *AJ*, 134, 2435
Willott C. J., et al., 2010, *AJ*, 139, 906
Wong K. C., et al., 2020, *MNRAS*, 498, 1420
Woods T. E., et al., 2019, *Publ. Astron. Soc. Australia*, 36, e027
Wu X.-B., et al., 2015, *Nature*, 518, 512
Wyithe J. S. B., Loeb A., 2002, *Nature*, 417, 923
Yang J., et al., 2016, *ApJ*, 829, 33
Yue M., Fan X., Yang J., Wang F., 2021, *ApJ*, 921, L27
Yue M., Fan X., Yang J., Wang F., 2022, *ApJ*, 925, 169

This paper has been typeset from a $\text{\TeX}/\text{\LaTeX}$ file prepared by the author.